NEUTRINO PHYSICS (NONACCELERATOR)

Y. TOTSUKA
Kamioka Observatory
Institute for Cosmic Ray Research,
The University of Tokyo
Higashi-Mozumi, Kamioka-cho, Yoshiki-gun,
Gifu 506-12, JAPAN

Nonaccelerator-based neutrino physics is reviewed. New experiments of atmospheric neutrinos clearly indicate that the observed ratio of muons to electrons is significantly smaller than what is expected. Moreover the zenith-angle distribution of atmospheric mu-neutrinos shows a strong distortion. A new experiment has observed too few solar neutrinos. The day-night effect was not observed within a few % level. The energy spectrum of solar neutrinos was indirectly measured but more data and better understanding of systematic uncertainties are needed for testing the neutrino-oscillation hypothesis. Reactor experiments are in progress and also double beta decays are actively being searched for.

1 Introduction

Neutrino experiments without usage of accelerators are the topics that I wish to cover. Their objectives are twofold ; (i) to study basic properties of neutrinos, especially their masses and mixings, (ii) to study deep interior of some astrophysical objects by using neutrinos as a probe. Tritium beta-decay experiments, which very precisely measure the end point of the beta-energy spectrum, have been carried out to search for a possible distortion of the Kurie plot that might be caused by a finite mass of electron-neutrino. Two experiments [1, 2] are still under way to reach the technological limit. The current upper limit of ν_e mass is less than 10 eV, though there is a subtle systematic effect that has caused the derived mass squared to be negative. The mass limit will be significantly lowered once this systematics is understood and removed. It is quite important to further improve the technique.

Double beta decay experiment is another way of searching for finite *Majorana* neutrino masses. If a nucleus of $(Z, N) = (2m, 2n)$, namely (even, even) is the lightest of all the nuclei with an equal mass number $Z + N$, three consecutive nuclei of $(Z, N) = (2m - 2, 2n + 2), (2m - 1, 2n + 1)$ and $(2m, 2n)$ in general have a mass sequence of $M(2m-1, 2n+1) > M(2m-2, 2n+2) > M(2m, 2n)$. The two even-even nuclei normally have spin-parity 0^+. Beta-decay $(2m - 2, 2n + 2) \rightarrow (2m - 1, 2n + 1) + e^- + \overline{\nu_e}$ is in this case energetically forbidden. Hence the nucleus $(2m-2, 2n+2)$ could decay into $(2m, 2n)$ by emitting two electrons simultaneously. In order for neutrinoless double beta-decay to occur, the neutrino must be of the *Majorana* type and massive (assuming that right-handed coupling is absent.) No evidence has yet been found for double beta-decay and the neutrino mass limit has reached 1 eV (68% C.L.) from an enriched ^{76}Ge experiment [3]. One needs a knowledge of the relevant nuclear matrix element to obtain the mass limit. It has been calculated by several groups, but the results were found to spread by almost an order of magnitude. Hence it is necessary to investigate a number of candidate nuclei such as ^{76}Ge, ^{82}Se, ^{100}Mo, etc. to dilute the theoretical uncertainties. It is important to improve the

experimental sensitivity and to reach the mass range of about 0.1 eV, which is inferred from the present atmospheric neutrino anomaly.

Neutrino oscillations take place only when the neutrinos have finite masses, as the appearance probability of $\nu_e \to \nu_\mu$, for example, is proportional to $\sin^2(\Delta m^2 L/4E)$ with the obvious notation. Note that one can measure only the mass squared difference in contrast to tritium beta-decay or double beta-decay experiments. In the non-accelerator regime three kinds of neutrino sources are being used; $\overline{\nu_e}$ from nuclear reactors, ν_e, $\overline{\nu_e}$, ν_μ, $\overline{\nu_\mu}$ from interactions of cosmic rays in the atmosphere (atmospheric neutrinos) and ν_e from nuclear fusion reactions in the Sun. (L, E), namely the typical distance of a neutrino source to a detector and the neutrino energy, are (1 km, 1$\sim$8 MeV), (10 $\sim$ 10^4 km, 0.5 $\sim$ 10 GeV) and (10^8 km, 0.2 $\sim$ 10 MeV) for reactor, atmospheric and solar neutrino experiments, respectively.

A new reactor experiment Kam-LAND [4] will extend the baseline L to 150 km, two orders of magnitude longer than the current experiments. Reactor experiments measure a possible change of the $\overline{\nu_e}$ flux at various L, namely the disappearance experiment. No one has tried to detect the neutral-current reactions.

Atmospheric neutrinos have been observed with large underground detectors. Observed events are classified as four types; (i) fully contained events in which all the tracks are contained in the detector and the incident neutrino energy is well estimated, (ii) partially contained events in which some of the tracks escape the detector and the visible energy is less than the incident one, (iii) upward through-going muons that are produced in the rock beneath the detector and pass through the detector, (iv) upward-going stopping muons that are also produced in the rock beneath the detector, enter and stop in the detector. Fully contained events are produced by low-energy neutrinos of a few 100 MeV $\sim$ a few 10 GeV, where the ratio $(\nu_\mu + \overline{\nu_\mu})/(\nu_e + \overline{\nu_e})$ is close to 2, as both $\pi^\pm$ produced high in the atmosphere and their daughter particles $\mu^\pm$ also decay out, resulting in the above ratio, which is insensitive to details of $\pi^\pm$ production mechanisms. Kamiokande [5] first announced an anomaly, namely, the ratio of the number of muons to that of electrons in the observed fully-contained sub-GeV data, N_μ/N_e, which is a good approximation to the ratio $(\nu_\mu + \overline{\nu_\mu})/(\nu_e + \overline{\nu_e})$, was found to be significantly smaller than what one expects. Two experiments with iron-calorimetric detectors, NUSEX [6] and Frejus [7] on the contrary obtained the ratio consistent with expectation, though their statistical significance was not very strong. The IMB water-Čerenkov experiment [8] later published the result on the N_μ/N_e ratio that was consistent with Kamiokande. Therefore the situation was a little controversial and more data were needed. Kamiokande [5] then analyzed the multi-GeV data and found that the zenith-angle distribution of the ratio N_μ/N_e did not agree with the expected one. Note that produced $\mu^\pm$ ($e^\pm$) closely follow the incident direction of ν_μ (ν_e) at these energies. If these results are indeed true, the most plausible explanation is that the neutrino oscillation takes place and ν_μ is converted to either ν_e or ν_τ. This year Super-Kamiokande and Soudan 2 [9] reported new results, though still preliminary, which are in good agreement with Kamiokande's observations both in the sub-GeV and multi-GeV ranges.

Upward-going muons provide additional information, since the relevant neutrino ener-

gies are much higher than those in the sub-GeV and multi-GeV ranges. One measures the total flux and zenith angle distribution. As for the multi-GeV case, the zenith angle is related to the baseline L, so that the shape of its distribution is sensitive to neutrino oscillation. Now MACRO [10], Kamiokande and Super-Kamiokande have a large enough number of upward-going muons for serious analyses. Their results seem to support the oscillation hypothesis but they must further be scrutinized.

It is now well established that there is a serious problem in solar neutrinos. All four experiments, Homestake [11], Kamiokande [12], SAGE [13] and GALLEX [14], observed much less neutrinos than what the standard solar models (SSM) predict. The question is now what is the solution to this solar neutrino problem. The most popular one is again the neutrino oscillation hypothesis which is indeed able to account for all the results obtained by the four experiments. The hypothesis then makes unique predictions ; (i) strong depletion of ^{7}Be neutrinos, (ii) distortion of the energy spectra of pp and ^{8}B neutrinos, (iii) apparent variation of the neutrino flux between daytime and nighttime, so called day-night effect, (iv) existence of neutrino species other than the original ν_e. New experiments were designed so as to challenge these predictions; Super-Kamiokande [15] for (ii) and (iii), SNO [16] for (ii), (iii) and (iv), Borexino [17] for (i). Super-Kamiokande presented the latested results on the observation of ^{8}B neutrinos, but more work is clearly needed to reduce systematic uncertainties. SNO will become operational in 1998 and Borexino hopefully in 1999. We will in a few years see a real solution to the solar neutrino problem.

Observation of solar neutrinos was initially intended to confirm nuclear fusion processes as the energy source in the Sun. This was indeed the first attempt to *see* deep interior of astrophysical objects by means of neutrinos. The four experiments, notably directional information obtained by Kamiokande, beautifully confirmed the nuclear energy production in the Sun. From the astrophysical point of view it is very important to monitor the solar-neutrino fluxes over many decades even after the solar neutrino problem has been solved.

The important astrophysical role of neutrinos was dramatically proven ten years ago by the successful observation of neutrinos from SN1987A, a supernova in the Large Magellanic Cloud, 160,000 light-years away. To watch supernovae in our galaxy is also very important and should be carried out for many decades or even centuries.

Search of ultra high-energy ($> 10^{12}$eV, UHE) extraterrestrial neutrinos will become a major field in coming years. It is an independent way to investigate what happens at active compact objects like pulsars, active galactic nuclei (AGN) . Evidence for neutrino emission will unambiguously demonstrate that charged pions are produced and hence UHE protons and nuclei are accelerated, namely a real discovery of the origin of cosmic rays. An under-water experiment in Lake Baikal [18] , has been operational to look for upward-going muons, but its effective area is too small even compared with the current underground detectors. AMANDA-B [19], which is an underice experiment at the South Pole, is ready and will provide the first result in 1998. The AMANDA experiment plans to extend the detector size large enough to obtain the first evidence for the existence of UHE astrophysical neutrinos.

So far I briefly summarized the present status of nonaccelerator-based neutrino physics. Now I discuss the latest results on atmospheric neutrinos in Chapter 2. Chapter 3 is for solar neutrinos. I then briefly present the current status of reactor experiments and double

beta decay experiments in Chapters 4 and 5, respectively. I conclude in Chapter 6.

2 Atmospheric Neutrinos

We follow Kamiokande [5] to categorize the observed event types; sub-GeV, multi-GeV, upward through-going muons and upward stopping muons. There is no new result on upward stopping muons and we will not discuss on them.

Experiments for atmospheric neutrinos observe electrons and muons and compare their numbers to the expected ones. To positively identify e and μ is not difficult. What is important is to reliably estimate the expected numbers from underlying theory. The observed number of events is given by

$$\frac{dN_\ell(\Theta, p_\ell)}{d\Omega_\Theta\, dp_\ell} = t_{obs} \sum_{\pm} \int N_t \frac{d\phi^{\pm}_{\nu_\ell}(E_\nu, \Theta)}{d\Omega_\Theta\, dE_\nu} \frac{d\sigma^{\pm}(E_\nu, p_\ell)}{dp_\ell} F(q^2) dE_\nu \qquad (1)$$

where ℓ stands for $e^{\pm}$ or $\mu^{\pm}$, p_ℓ the lepton momentum, E_ν the neutrino energy, θ the zenith angle, t_{obs} the observation time, N_t the number of target particles, $\phi_{\nu_\ell}(E_\nu, \Theta)$ the neutrino flux, $\sigma(E_\nu, p_\ell)$ the cross section. $F(q^2)$ takes into account the nuclear effects like Fermi-momenta of target nucleons, Pauli blocking of recoil nucleons and so on. The summation ($\pm$) is done for ν_ℓ and $\overline{\nu_\ell}$, since observations do not distinguish the lepton charge. The neutrino fluxes $\phi_{\nu_\ell}(E_\nu, \Theta)$ have been calculated most recently by the Bartol group [20] and the ICRR group [21]. Both calculations agree reasonably well (within 10 % for 200 MeV $< E_\nu <$100 GeV) [22] but there still exist 20 % uncertainties in the absolute fluxes owing mostly to the absolute flux of primary cosmic rays. Solar activities and geomagnetic fields affect the low-energy side of the fluxes and they have been properly treated in the calculations.

The cross sections $\sigma^{\pm}(E_\nu, p_\ell)$ have charged-current (CC) and neutral-current (NC) contributions each of which is further classified as quasi-elastic (qe), 1π production (1π) and multi-π($m\pi$) production. Their uncertainties are as large as those for the fluxes. Fortunately thanks to the lepton universality uncertainties in $\phi_\nu \times \sigma$ largely cancel when the ratio N_μ/N_e is taken. The estimated uncertainties are listed in Table 1. Note however that the uncertainties in N_ℓ depend on experimental procedures. For example, in the sub-GeV energy range, experiments normally pick up one- or two- prong events which are dominated by the CC_{qe} channel and correspondingly have less uncertainties. The nuclear effects must be properly taken into account, since the targets are water or iron. An example of their treatment is shown in table 2. The effects are important only in the low-energy region.

Now let us discuss the results on sub-GeV, multi-GeV and upward through-going muons.

2.1 $R \equiv (N_\mu/N_e)_{data}/(N_\mu/N_e)_{MC}$

There are four experiments, Kamiokande [5], NUSEX [6], Frejus [7] and IMB [8] that have published the results. They are normally expressed by the double ratio $R \equiv (N_\mu/N_e)_{data}$ $/(N_\mu/N_e)_{MC}$, namely the observed ratio divided by the expected one in order to cancel

Table 1: Effects of uncertainties in the neutrino cross sections on e-like yields, μ-like yields and the ratio N_μ/N_e in the sub-GeV region (for Super-Kamiokande). The sub-GeV energy range is defined as 100 MeV/c - 1330 MeV/c for e-like events and 200 MeV/c - 1330 MeV/c *visible momentum* for μ-like events respectively. The visible momentum of 1330 MeV/c approximately corresponds to a muon momentum of 1400 MeV/c.

modes	e-like	μ-like	N_μ/N_e
CC_{qe}:			
change M_A^a by +10 %	+4.6 %	+5.4 %	+0.8 %
change M_A by −10 %	−4.7	−5.5 %	−0.9 %
$CC_{1\pi} + CC_{m\pi}$:			
change σ by +30 %	+6.2 %	+6.1 %	−0.2 %[b]
change σ by −30 %	−6.2 %	−6.1 %	+0.2 %
$NC_{1\pi} + NC_{m\pi}$:			
change σ by +50 %	+4.0 %	+1.9 %	−2.0 %
change σ by −50 %	−4.0 %	−1.9 %	+2.2 %

[a] Axial vector mass, $M_A = 1.01$ GeV.
[b] Dominated by statistical errors of simulated data.

Table 2: Effects of uncertainties in the nuclear effects on e-like yields, μ-like yields and the ratio N_μ/N_e in the sub-GeV region (for Super-Kamiokande).

models	e-like	μ-like	N_μ/N_e
Fermi-gas model:			
change p_F to 180 MeV/c[a]	+12.3 %	+8.4 %	−3.4 %
Binding energy of p, n:			
change from off to on[b]	−1.9 %	−1.4 %	+0.6 %

[a] Fermi momentum, nominal value is 250 MeV/c.
[b] on(off), binding effect(not) considered. $p_F = 217$ MeV/c.

the $\phi_\nu \times \sigma$ uncertainties. The uncertainties caused by the cross sections and nuclear effects are estimated to be $\leq 3.6\%$ and $\leq 3\%$ for CC and NC reactions respectively, i.e., small numbers thanks to the cancellation. The experimental results are summarized in table 3, in which the range of observed momenta and the exposure ($N_t \times t_{obs}$ in eq(1) in units of kt·yr) are shown. Note that the observed number of events is approximately proportional to the exposure. As one sees, Frejus and NUSEX, both employing fine-grain iron-calorimeters, obtained the results consistent with expectation, while Kamiokande and IMB with large water-Čerenkov detectors observed significantly smaller R than expected.

New experiments, Soudan 2 [9] and Super-Kamiokande [23], reported the new results as shown in Table 3 and confirmed the small R.

Some comments are in order:

(i) The most important technique here is to identify e and μ. Both experimental groups with water-Čerenkov and fine-gain detectors tested and confirmed the e/μ identification (ID) ca-

Table 3: Results on R. p_ℓ denotes the momentum range of observed charged leptons (Kamiokande, IMB and Super-Kamiokande) or of observed events (Frejus, NUSEX and Soudan 2). Exposure is a measure of the observed number of events and corresponds to $N_t \cdot t_{obs}$ in eq(1). Note that the low-energy (high-energy) result of Kamiokande and Super-Kamiokande is called sub-GeV (multi-GeV). Event selections are different among experiments.

Experiments	p_ℓ(MeV/c)	Exposure (kt·yr)	R	Ref.
Kamiokande	$\begin{pmatrix} e{:}100-1330 \\ \mu{:}200-1400 \end{pmatrix}$	7.7	$0.60^{+0.06}_{-0.05} \pm 0.05$	[5]
	$\begin{pmatrix} e{:}1330- \\ \mu{:}1400- \end{pmatrix}$	$6.0 \sim 8.2$	$0.57^{+0.08}_{-0.07} \pm 0.07$	[5]
IMB	$\begin{pmatrix} e{:}100-1500 \\ \mu{:}300-1500 \end{pmatrix}$	7.7	$0.54 \pm 0.05 \pm 0.12$	[8]
Frejus	$\begin{pmatrix} e{:}200- \\ \mu{:}200- \end{pmatrix}$	2.0	$1.00 \pm 0.15 \pm 0.08$	[7]
NUSEX	$\begin{pmatrix} e{:}200- \\ \mu{:}200- \end{pmatrix}$	0.74	$0.99^{+0.35}_{-0.25}$	[6]
Soudan 2	$\begin{pmatrix} e{:}150- \\ \mu{:}100- \end{pmatrix}$	2.83	$0.61 \pm 0.14^{+0.05}_{-0.07}$	[9]
Super-Kamiokande	$\begin{pmatrix} e{:}100-1330 \\ \mu{:}200-1400 \end{pmatrix}$	20	$0.635 \pm 0.033 \pm 0.053$	[23]
	$\begin{pmatrix} e{:}1330- \\ \mu{:}1400- \end{pmatrix}$	$18 \sim 20$	$0.604^{+0.065}_{-0.058} \pm 0.067$	[23]

pabilities with accelerator test beams. The mis-ID probabilities are smaller than several %, depending on experiments. Especially Kamiokande and Super-Kamiokande claim that the mis-ID probability is less than 2% [54] and hence it never causes the small R.
(ii) It is unlikely that the nuclear effects reduce the double ratio R from 1 to about 0.6 as seen in table 2. The effect comes in R only from the muon mass and becomes very small for visible energies above a few hundred MeV, and in fact negligible in the multi-GeV range, while Kamiokande and Super-Kamiokande still observed a strong reduction of R there.
(iii) The Soudan 2 detector has a capability of determining the track directionality, otherwise is similar with Frejus' fine-grain detector. It is very important that it still continues observation and makes the result statistically more solid. Based on the new results, it can be said that the small R is now established. Figure 1 shows R as a function of p_ℓ for fully-contained data obtained by Super-Kamiokande.

2.2 Zenith Angle Distribution

The higher the neutrino energy, the better the produced e/μ follows the neutrino direction. As discussed in Chapter 1, the zenith angle is a direct measure of its flight length L, and hence neutrino oscillation may manifest itself as a possible distortion of the zenith angle distribution. Since the shape itself does not depend on uncertainties in the absolute fluxes or cross sections, it is a sensitive way to search for the neutrino oscillation.

Kamiokande [5] published the zenith angle distribution of the double ratio R, which apparently did not follow the expected shape. Now Super-Kamiokande has 2.5 times as many events as Kamiokande. Figure 2 shows the zenith angle distributions of multi-GeV e-like and μ-like events obtained by Super-Kamiokande. Also shown is $dR(\Theta)/d\cos\Theta$ together

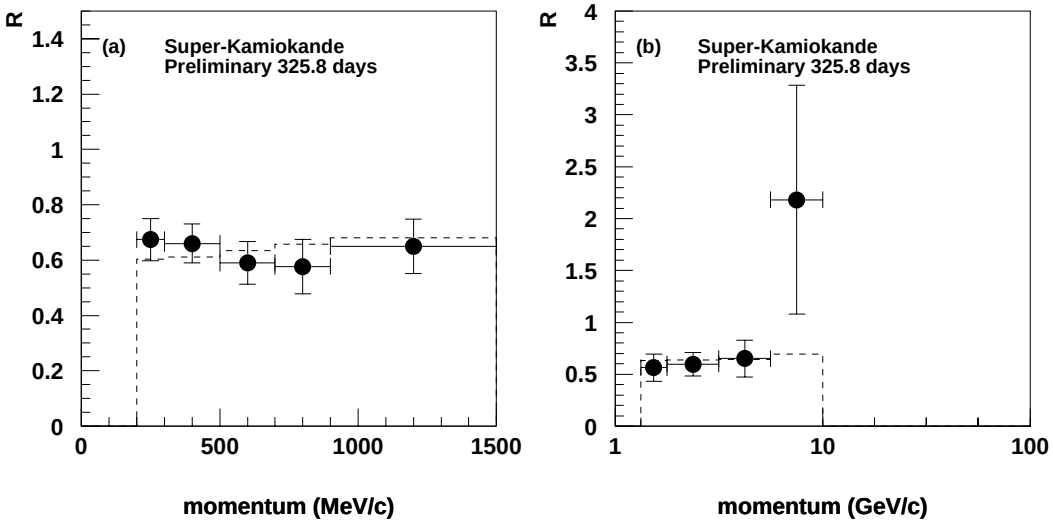

Figure 1: $R\,vs\,p_\ell$ for fully-contained events observed in the Super-Kamiokande detector. (a) for sub-GeV 1-ring events and (b) for multi-GeV 1-ring events. Dashed lines represent $R\,vs\,p_\ell$ expected from the assumption of $\nu_\mu - \nu_\tau$ oscillation with $\Delta m^2 = 5 \times 10^{-3}\,\mathrm{eV}^2$ and $\sin^2 2\theta = 1$.

with the Kamiokande result. Though the new result on $dR(\Theta)/d\cos\Theta$ has a more modest distortion than Kamiokande's, it is clear that there are less μ-like events in the upward direction (long L) than expected while the number of downward-going μ-like events (short L) is consistent with the expectation. The distortion is less visible in the e-like events. Hence $dR(\Theta)/d\cos\Theta$ largely reflects the μ-like distribution.

Something interesting is indeed happening there.

2.3 Upward Through-going Muons (thru-muons)

These muons are selected (i) by detecting entering and exiting points in the detector and (ii) by requiring their track lengths longer than a preset length L_{min} corresponding to a minimum energy E_{min}. Normally track lengths of thru-muons in a detector are longer than L_{min} due to the constraint of through-going. Therefore the detection efficiency in general increases from E_{min} and reaches the plateau at an energy E_{max} which is higher than E_{min}, and E_{max} depends on the detector geometry.

Upward stopping muons (stop-muons) have energies just between E_{min} and E_{max}, and improve the efficiency curve to almost a step function. However selection of the stop-muons is not easy and reliable results are not available yet, though Super-Kamiokande will soon provide the first result.

Figure 3 shows the energy distribution of atmospheric mu-neutrinos that would produce thru-muons and stop-muons in the Super-Kamiokande detector. It is seen that parent neutrinos of thru-muons have much higher energies ($< E_\nu > \sim$ 100 GeV) than those that produce sub-GeV or multi-GeV events. Therefore these muons will provide new and independent information which may shed new light on the origin of the small R and distorted

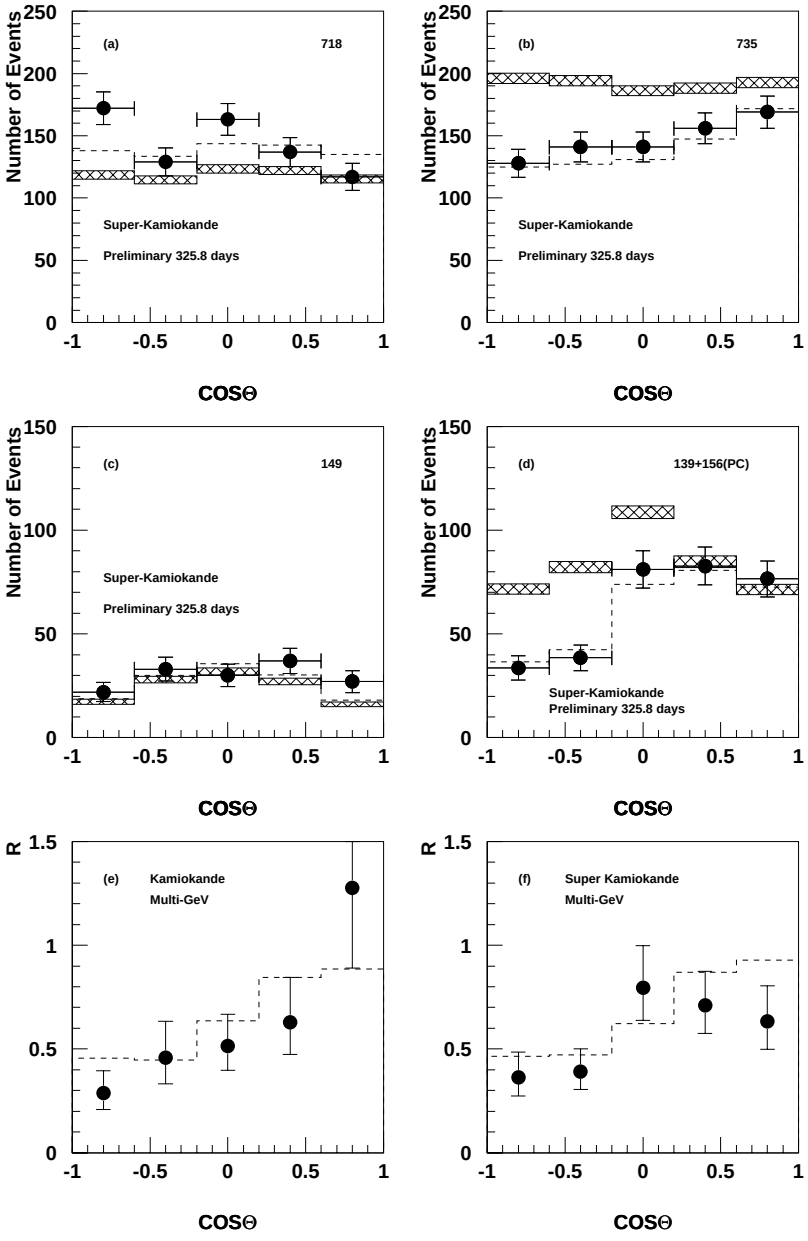

Figure 2: Zenith angle ($\cos\Theta$) distributions observed in Super-Kamiokande. (a) electron-like sub-GeV fully-contained 1-ring events corresponding to 326 day observation (718 events). Crossed bands are those expected from no oscillation hypothesis and their widths are statistical accuracy of the Monte Carlo simulation. The dashed lines indicate those expected from the assumption of $\nu_\mu - \nu_\tau$ oscillation with $\Delta m^2 = 5 \times 10^{-3}\,\mathrm{eV}^2$ and $\sin^2 2\theta = 1$. (b) same as (a) for muon-like sub-GeV fully-contained 1-ring events (326 day, 735 events). (c) same as (a) for electron-like multi-GeV fully-contained events (326 day, 149 events). (d) same as (a) for muon-like multi-GeV fully-contained events (326 day, 139 events) plus partially-contained events (293 day, 156 events). (e) Multi-GeV R observed in Kamiokande[5]. (f) same as (e) for Super-Kamiokande.

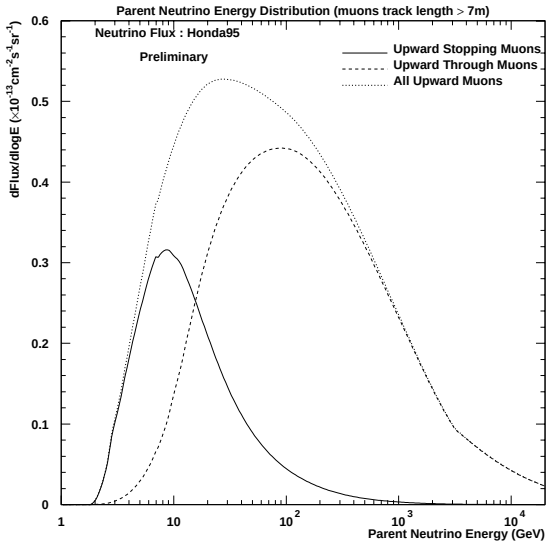

Figure 3: Energy distribution of parent mu-neutrinos that would produce upward through-going (dashed line) and stopping (solid line) muons. They were calculated for the Super-Kamiokande detector but do not sensitively depend on the detector geometry. The dotted line is a sum of the two. The original neutrino flux was adopted from Honda et al. [21] and the parton distribution function from (GRV94DIS) [25].

zenith angle distribution.

Now let us discuss the new results. Table 4 presents the results from Kamiokande [24], MACRO [10] and Super-Kamiokande [23]. MACRO is a large underground detector with a size of 12m(W) $\times$ 77m(L) $\times$ 9.5m(H) located in Gran Sasso. It consists of tracking detectors and scintillation counters. Direction of muons is determined by the time-of-flight information from the scintillation counters. MACRO has an excellent detection efficiency for near-vertical (up and down) muons but the efficiency decreases rapidly as the muon direction becomes horizontal. The detector, however, is thinner than Kamiokande or Super-Kamiokande, and E_{min} is correspondingly smaller. The flux of thru-muons is calculated as

$$\frac{dF(\Theta, E_\mu)}{d\Omega_\Theta\, dE_\mu} = N_A \sum_{\pm} \int_{E_{min}}^{\infty} dE_\nu \frac{d\phi^{\pm}_{\nu_\mu}(E_\nu, \Theta)}{d\Omega_\Theta\, dE_\nu} \int_{E_{min}}^{\infty} dE'_\mu \frac{d\sigma^{\pm}(E_\nu, E'_\mu)}{dE'_\mu} \times$$

$$\times \int_0^{\infty} dL P_\mu(E'_\mu, E_\mu, L), \qquad (2)$$

where N_A is Avogadro's number, $\phi^{\pm}_{\nu_\mu}$ and $\sigma^{\pm}$ the same as in eq(1) and P_μ the survival probability of a muon that had the initial energy of E'_μ and still has an energy (E_μ, $E_\mu + dE_\mu$) after traversal of a distance L. P_μ depends on the range-energy relation and its struggling.

Table 4: New results on upward through-going muons from Kamiokande, MACRO and Super-Kamiokande

Experiments	Detection [a] Area(m^2)	E_{min} (GeV)	number of observed muons	expected number	Ref.
Kamiokande	150	1.7	373 ± 19	414 ± 83	[24]
MACRO	900	1.0	$350 \pm 19 \pm 28$	472 ± 80	[10]
Super-Kamiokande	1100	1.7	409 ± 20	445 ± 89	[23]

[a] only approximate numbers

The observed number of thru-muons is then,

$$N_\mu(E_{min}) = t_{obs} \int_{E_{min}}^{\infty} dE_\mu \int d\Omega_\Theta \frac{dF(\Theta, E_\mu)}{d\Omega_\Theta \, dE_\mu} \, S(\Theta)|_{through} \tag{3}$$

where $S(\Theta)$ is the detector area and the integration must be carried out under the condition of through-going. The calculated results are shown in the last column of table 4. The calculational uncertainties are still large, about 20 %, and are dominated by unknowns in ϕ_ν. Hence direct confrontation with observed results is not very meaningful. Results from Kamokande and Super-Kamiokande are consistent with the expected numbers within 1σ, while MACRO saw fewer muons, about $1.5\,\sigma$ below. Note that MACRO's observed events are mostly vertically upward ($\cos\Theta \approx -1$) due to strong angular dependence of the detection efficiency.

Figure 4 shows zenith angle distributions obtained by the three experiments. One immediately sees that the MACRO data do not fit the theoretical curve very well, even if one makes the absolute-flux constraint completely free. The shape itself looks different. Note that the shape of the zenith angle distribution is independent of the absolute flux like the ratio N_μ/N_e and can be calculated with little uncertainty. Kamiokande and Super-Kamiokande did not see such a large deficit as shown in the figure. One must study if the three results at $\cos\Theta \approx -1$ are really in conflict each other. Nevertheless the observed data seem not to follow the calculated shape. The three experimental groups obviously need more quantitative study.

2.4 Possible Neutrino Oscillations

Experiments have revealed the small R in the sub-GeV and multi-GeV regions, the deformed zenith angle distribution in the multi-GeV region and possibly the deformed zenith angle distribution in the upward through-going muons. Although more data are certainly desirable, one has to seriously consider what causes these discrepancies. Neutrino oscillation may be a solution to them and may well be the unique one.

Super-Kamiokande made an analysis of the sub-GeV and multi-GeV data assuming the $\nu_\mu - \nu_\tau$ oscillation. A preliminary result is shown, namely the allowed region in the $(\Delta m^2, \sin^2 2\theta)$ plane, in Fig.5 together with Kamiokande's old result (allowed region) and other results (excluded regions). The allowed region is in $\Delta m^2 = 10^{-3} \sim 10^{-2}\,\mathrm{eV}^2$ and has only a small overlap with Kamiokande's result. The curves in Figs.1, 2 and 4 (except

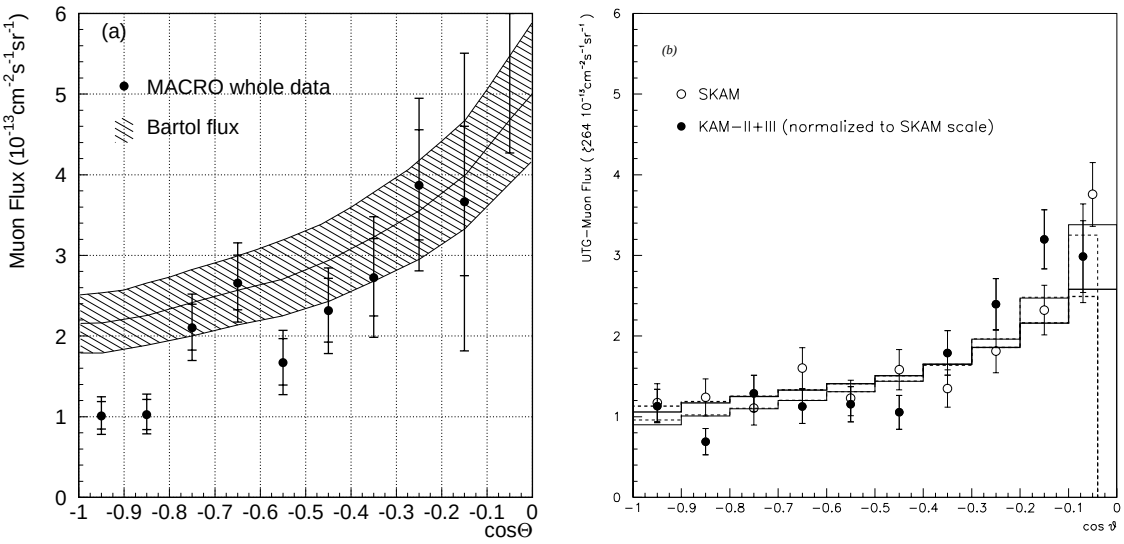

Figure 4: Zenith angle ($\cos\Theta$) distributions of upward through-going muons observed by MACRO, Kamiokande and Super-Kamiokande. (a) MACRO results compared with the expected distribution calculated with the Bartol flux[20]. (b) Kamiokande (full circle) and Super-Kamiokande (open circle) results with the expected distributions from no oscillation (thick solid and dashed lines for Super-Kamiokande and Kamiokande, respectively) and from $\nu_\mu - \nu_\tau$ oscillation with $\Delta m^2 = 5 \times 10^{-3}\,\mathrm{eV}^2$ and $\sin^2 2\theta = 1$ (thin solid and dashed lines for Super-Kamiokande and Kamiokande, respectively). The results and expected lines for Kamiokande were multiplied by a factor 0.819 to scale its geometrical effect to Super-Kamiokande. The expected lines are the best fitted ones obtained within the absolute scale uncertainty of 20%.

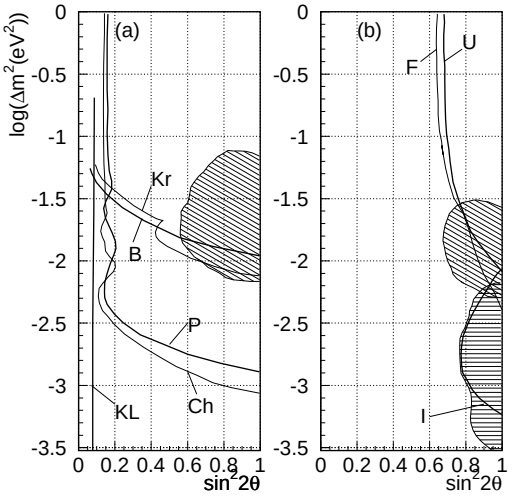

Figure 5: Allowed regions (90 % CL) in the (Δm^2, $\sin^2 2\theta$) space. (a) for $\nu_\mu - \nu_e$ oscillation and (b) for $\nu_\mu - \nu_\tau$ oscillation. Regions with slanting lines indicate the allowed regions obtained by Kamiokande [5]. A horizontally hatched region in (b) is the preliminary allowed region by Super-Kamiokande. Other lines show that their upper-right sides are excluded; B, Bugey reactor experiment [26]; Kr, Krasnoyarsk reactor experiment [27]; F, Frejus fully-contained atmospheric neutrinos [7]; U, compilation of old upward through-going muons [28]; I, IMB upward stopping muons [29]. Super-Kamiokande's analysis on $\nu_\mu - \nu_e$ oscillation was not ready. Also shown are the expected sensitivities from reactor experiments denoted as Ch, Chooz [30]; P, Palo Verde [31]; KL, Kam-LAND [10] (See chapter 4 for details).

MACRO) are those that have been calculated under the assumption of $\nu_\mu - \nu_\tau$ oscillations with $\Delta m^2 = 5 \times 10^{-3}\,\mathrm{eV}^2$ and $\sin^2 2\theta = 1$. They nicely explain the various characteristics.

More systematic studies are being undertaken and interesting results will soon come out.

3 Solar Neutrinos

3.1 Neutrino Fluxes on Earth

Some characteristics on the main sources of solar neutrinos are listed in table 5. Electron neutrinos from those three sources are called *pp*, ^{7}Be and ^{8}B neutrinos, respectively. Other sources (*pep*, *hep*, ^{13}N, ^{15}O, ^{17}F) do not significantly contribute to observations. It has been argued that the flux estimate of ^{8}B neutrinos should have large uncertainties and the error given in table 5 is too small. Recently, however, helioseismology has made great progress and begins to impose strong constraints on solar model calculations.

The basic equations that control the inside of the Sun are:

$$\frac{dM_r}{dr} = 4\pi r^2 \rho, \tag{4}$$

$$\frac{dP(r)}{dr} = -\frac{GM_r\rho}{r^2}, \tag{5}$$

Table 5: Main sources of solar neutrinos

Sources	E_ν(MeV)	Flux on Earth ($10^{10}\,\mathrm{cm^{-2}s^{-1}}$)[a]
$pp \rightarrow de^+\nu_e$	≤ 0.420	5.91 ± 0.06
$^7\mathrm{Be}(\nu_e, e)^7\mathrm{Li}$	$0.862(89.7\,\%)$[b] $0.384(10.3\,\%)$	$0.515^{+0.31}_{-0.36}$
$^8\mathrm{B} \rightarrow ^8\mathrm{Be}^* e^+\nu_e$	≤ 15[c]	$(6.62^{+0.93}_{-1.13}) \times 10^{-4}$

[a] Integrated fluxes shown are the ones calculated by Bahcall and Pinsonneault. [34]

[b] Line spectra.

[c] Spectrum shape is influenced by a broad decay width of the excited state $^8\mathrm{B}^*(J^P = 2^+)$.

$$\frac{dL_r}{dr} = 4\pi r^2 \rho(\varepsilon + \varepsilon_g) \tag{6}$$

$$\frac{dT}{dr} = \begin{cases} -\frac{3}{4ac}\frac{\kappa\rho}{T^3}\frac{L_r}{4\pi r^2} & if\ radiative \\ (dT/dr)_{conv} & if\ convective \end{cases} \tag{7}$$

where M_r is the internal mass within the radius r, $P(r)$ the pressure, L_r the internal luminosity generated within the radius r, T the temperature, κ the opacity, and a the Stefan-Boltzmann constant. ε and ε_g are the nuclear and gravitational energy generation rates. One further needs an auxiliary equation, namely the equation of state. If all atoms are completely ionized, it is simply

$$P = \rho\frac{kT}{\mu m_H}, \tag{8}$$

where μ and m_H are the mean molecular weight and hydrogen mass, respectively. $\mu^{-1} = X + \frac{3}{4}Y + \frac{1}{2}Z$; X, Y and Z being the mass fractions of hydrogen, helium and heavier elements, respectively. Since the chemical abundance in the Sun evolves in time as a result of nuclear fusion reactions, one has to solve the basic equations over the entire solar history and estimate the present X, Y and Z as a function of the radius.

Helioseismology now provides an additional equation. Crudely speaking, it is

$$c^2(r) = k\frac{P}{\rho}, \tag{9}$$

where $c(r)$ is the sound velocity at the radius r and k is a constant. Helioseismology determines $c(r)$ very precisely over the range of r from the solar surface to the innermost region of $r \leq 0.05R_\odot$. In this case, without integrating the equations over the history of the Sun, T/μ can be obtained as a function of r with the help of eq(8). The basic equations are then solved with the boundary conditions: $L_r(0) = M_r(0) = 0$, $L_r(R_\odot) = L_\odot$ and $M_r(R_\odot) = M_\odot$. In reality things are much more complicated, and additional assumptions

Table 6: Helioseismology-inspired calculations of the ^{7}Be and ^{8}B neutrino fluxes. The first and second errors in each calculation correspond to uncertainties from helioseismology and nuclear cross sections, respectively.

	S	R	$BP95$
^{7}Be(10^{10}cm^{-2}s^{-1})	$5.29^{+0.37}_{-0.55} \pm 0.28$	$4.81 \pm 0.53 \pm 0.20$	$5.15 \pm^{+0.31}_{-0.36}$
^{8}B(10^6cm^{-2}s^{-1})	$6.74^{+0.93}_{-1.26} \pm 0.72$	$5.96 \pm 1.49 \pm 0.64$	$6.62^{+0.93}_{-1.13}$

S M. Takita and H. Shibahashi [32];
R B. Ricci, V. Berezinsky, S. Degl'Innocenti, W.A. Dziembowski and G. Fiorentini [33];
$BP95$ J.N. Bahcall and M.H. Pinsonneault [34].

are needed. One must also input the nuclear cross section factors and the opacity. Nevertheless helioseismology puts a strong constraint on the neutrino fluxes. Table 6 shows two helioseismology-inspired calculations [32, 33], which are compared with a standard calculation done by Bahcall and Pinsonnealt [34]. The agreement is excellent and confirms the validity of the standard calculations.

3.2 Observed Rates

It is well know that all the four experiments (Homestake [11], SAGE [13], GALLEX [14] and Kamiokande [12]) saw fewer neutrino events than expected.

Kamiokande was terminated in 1995. But a 50,000 ton water Čerenkov detector, Super-Kamiokande, became operational in April 1996. Its detector characteristics are more or less the same as Kamiokande, but low-energy backgrounds have been reduced by almost two orders of magnitude and the energy resolution has also been improved. Super-Kamiokande reported the preliminary results based on 306-day observation.

Homestake, SAGE and GALLEX are radiochemical experiments, in which target atoms (atomic number Z) interact with solar neutrinos and transmute themselves into new radioactive atoms ($Z+1$). These atoms have relatively long lifetimes and go back to the original atoms via electron capture. Their production rates are about $1 \sim 2$ atoms/day, purely determined by detector sizes. SAGE reported a new but preliminary result.

A new 1,000 t heavy-water Čerenkov detector SNO [16] is in the last stage of construction. It is expected to become operational early next year. Another ambitious experiment Borexino [17] is a 300 t liquid scintillation detector. Its unique feature is a very low threshold energy, a few 100 keV and is capable of detecting ^{7}Be neutrinos (0.86 MeV) via $\nu_e e \to \nu_e e$ with a counting rate of 50 events/day (fiducial mass =100 t).

Some features of the current and near-future detectors are listed in table 7. Results from the five experiments are shown in table 8 together with expected numbers. It is obvious that all the results show significant deficits of solar neutrinos, so called the solar neutrino problem.

Some comments are in order.

(1) GALLEX [35] and SAGE [36] carried out ^{51}Cr source experiments. ^{51}Cr decays via elec-

Table 7: Current and Future experiments

Experiments	Reactions	E_{th}(MeV)[a]	Remarks
Homestake	$^{37}\mathrm{Cl}(\nu_e, e)^{37}\mathrm{Ar}$	0.814	Radiochemical
SAGE/GALLEX	$^{71}\mathrm{Ga}(\nu_e, e)^{71}\mathrm{Ge}$	0.233	Radiochemical
Kamiokande	$e(\nu_e, e)\nu_e$	6.5	Counting
Super-Kamiokande	$e(\nu_e, e)\nu_e$	6.0	Counting
BOREXINO	$e(\nu_e, e)\nu_e$	0.25	Counting
SNO	$d(\nu_e, e)2p$	~ 5	Counting
	$d(\nu_e, \nu_e)pn$	2.225	Counting

[a]Minimum detectable neutrino energy

Table 8: Results on solar neutrinos

Experiments	Results	Expected[a]	Remarks	Ref.
Homestake	$2.54 \pm 0.16 \pm 0.14$ SNU	$9.3^{+1.2}_{-1.4}$ SNU		[11]
SAGE	$73 \pm 8.5^{+5.2}_{-6.9}$ SNU	137^{+8}_{-7} SNU	new, preliminary	[13]
GALLEX	$69.7 \pm 6.7^{+3.9}_{-4.5}$ SNU	137^{+8}_{-7} SNU		[14]
Kamiokande	$2.80 \pm 0.19 \pm 0.33$ $\times 10^6 \mathrm{cm}^{-2}\mathrm{s}^{-1}$	$6.62^{+0.93}_{-1.13}$ $\times 10^6 \mathrm{cm}^{-2}\mathrm{s}^{-1}$	^{8}B flux	[12]
Super-Kamiokande	$2.44 \pm 0.06^{+0.25}_{-0.09}$ $\times 10^6 \mathrm{cm}^{-2}\mathrm{s}^{-1}$	$6.62^{+0.93}_{-1.13}$ $\times 10^6 \mathrm{cm}^{-2}\mathrm{s}^{-1}$	new, preliminary	[23]

[a]Calculated by Bahcall and Pinsonneault [34].

tron capture ($t_{1/2} = 27.7\,days$) and emits gamma rays of 0.751 MeV (90 %) and 0.426 MeV (10%). The sources of very high radioactivity were inserted in the ^{71}Ga tanks and ^{71}Ge yields were measured. Knowing the absolute neutrino intensity of the sources, both groups obtained the ratio 'measured/predicted'. GALLEX carried it out twice and obtained the ratio 0.97 ± 0.11 and 0.83 ± 0.10 with the combined result 0.92 ± 0.08. SAGE did it once and the measured ratio was 0.95 ± 0.11. The results are consistent with the expected ones and proved that the underlying technique is right and reliable.

(2) Super-Kamiokande's central value is smaller than Kamiokande's. It may be due to a difference of the energy calibrations. Kamiokande used gamma rays from Ni(n,γ)Ni and compared the observed number of hit photomultiplier tubes (PMTs) with the simulation, while Super-Kamiokande used electrons from a LINAC with energies $5 \sim 16$ MeV. There seems to exist unknown systematics in the Ni(n,γ)Ni calibration. This problem is still under study.

(3) Based on recent helioseismological data, it is unlikely that the standard solar model

has a gross overestimate of the ^{8}B neutrino flux. The discrepancy between observation and calculation of the ^{8}B neutrino flux is indeed serious.
(4) Cumming and Haxton [37] recently proposed a non-standard solar model which might explain a large deficit of ^{7}Be neutrinos but yet a reasonable flux of ^{8}B neutrinos. Their scenario roughly goes in the following way.

^{3}He nuclei are produced by the reaction $d(p, \gamma)^3$He and are normally concentrated in the region $r \simeq 0.2 \sim 0.4 R_\odot$. Let us assume that the ^{3}He-rich material diffuses downward to the core in a time interval sufficiently short that it is not burned during downward moving. As soon as ^{3}He reaches the region $r \simeq 0.05 R_\odot$, it is suddenly ignited. Since the temperature is much higher there than in the normal equilibrium region, the two competing reactions (^{3}He(^{3}He, $2p$)^{4}He and ^{3}He(^{4}He, γ)^{7}Be) change their rates. The first reaction dominates and the ^{7}Be production is strongly inhibited, resulting in fewer ^{7}Be neutrinos. On the other hand the reaction ^{7}Be$(p, \gamma)^8$B goes rapidly thanks to a high temperature and a reasonable amount of ^{8}B neutrinos are produced. Note that Kamiokande observes only ^{8}B neutrinos and relative contributions to Homestake's event rate are $^8\mathrm{B} : {}^7\mathrm{Be} : others = 7.36 : 1.24 : 0.7$ SNU according to SSM. Cumming and Haxton's model could reduce ^{8}B and ^{7}Be neutrinos to 40 % and 30 %, respectively, compared to SSM, and explain the results from Kamiokande ($data/SSM \approx 40\,\%$) and Homestake ($data/SSM \approx 30\,\%$).

However, Bahcall and Pinsonneault [38] criticized that the model predicts the sound spreed profile which does not agree with the one measured by helioseismology. Also mechanism of the large ^{3}He mixing is not known.

3.3 Day-Night Effect and Energy Spectrum

Counting experiment is able to obtain additional information. It is well known that if the neutrino oscillation is indeed the solution to the solar neutrino problem [39,40], one expects rather exotic phenomena. (i) The event rate in the nighttime could be larger than in the daytime, namely the day-night effect. Oscillated neutrinos (ν_μ *or* ν_τ) inside the Sun could have a finite chance to be reconverted to the original ν_e in Earth. This would lead to a larger event rate in the nighttime.

Kamiokande published the negative result on the day-night effect. Super-Kamiokande reported a new result which indicates no effect within experimental uncertainties;

$$\frac{D-N}{D+N} = -0.017 \pm 0.026(stat.) \pm 0.017(syst.), \tag{10}$$

where D and N stand for daytime and nighttime event rates respectively. This result is based on 306 day data, $E_e = 6.5 - 20$ MeV (note E_e is the kinetic but total energy) and 22.5 kton fiducial volume. (ii) The neutrino energy spectrum could be distorted. Again Super-Kamiokande reported the first result on the energy spectrum of recoil electrons, which is reproduced in Fig.6 in which the ratio data/SSM (the number of observed events divided by the corresponding one from SSM) is plotted against E_e. If there is no spectral distortion, the data/SSM should be flat. Unfortunately statistical and systematic errors are still too large for the result to be meaningful. The systematic errors are dominated by calibration and they will be reduced significantly once the detector is understood properly.

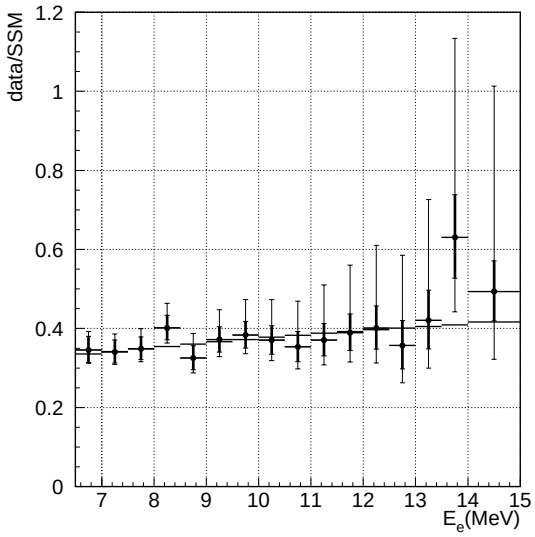

Figure 6: Data/SSM (number of observed events/corresponding number expected from SSM) vs electron (total) energy obtained by Super-Kamiokande. Thick (thin) error bars correspond to statistical (systematic) ones. The results are preliminary. The curve indicates what one expects from the MSW small-angle solution ($\Delta m^2 = 6 \times 10^{-6}\,\mathrm{eV}^2$, $\sin^2 2\theta = 7.0 \times 10^{-3}$).

It is nevertheless interesting to compare the data with what one expects from the MSW scenario. Figure 6 also shows an expected curve from the large-angle MSW solution ($\Delta m^2 = 6 \times 10^{-6}\mathrm{eV}^2$,$\sin^2 2\theta = 7.0 \times 10^{-3}$). It is certainly a good fit !

3.4 Possible Solution to the Solar Neutrino Problem

From the arguments given above, neutrino oscillation is the best candidate to solve the solar neutrino problem. Hata and Langacher [41] made a detailed analysis of the existing data and derived the three allowed regions in the (Δm^2, $\sin^2 2\theta$) space which is shown in fig.7. Also shown is an excluded region obtained from Super-Kamiokande's result on the day-night effect. Future experiments may very well find the unique solution by precisely measuring the neutrino energy spectrum, day-night effect, seasonal variation and NC reactions. We have already shown in Fig.6 how the MSW small-angle solution affects the energy spectrum that will soon be tested by Super-Kamiokande.

4 Reactor Neutrinos

Anti-electron neutrinos ($\overline{\nu_e}$) are produced from beta decays of neutron-rich nuclei which are fragments from nuclear fissions in a reactor. Commercial reactors these days have typical thermal power of multi GW, and are very strong $\overline{\nu_e}$ sources, resulting in neutrino fluxes exceeding $10^{10}\mathrm{cm}^{-2}\mathrm{s}^{-1}$ at a detector site. These intense neutrinos have been used to search for neutrino oscillations.

Reactor neutrinos have a continuous energy spectrum extending to about 8 MeV. Ex-

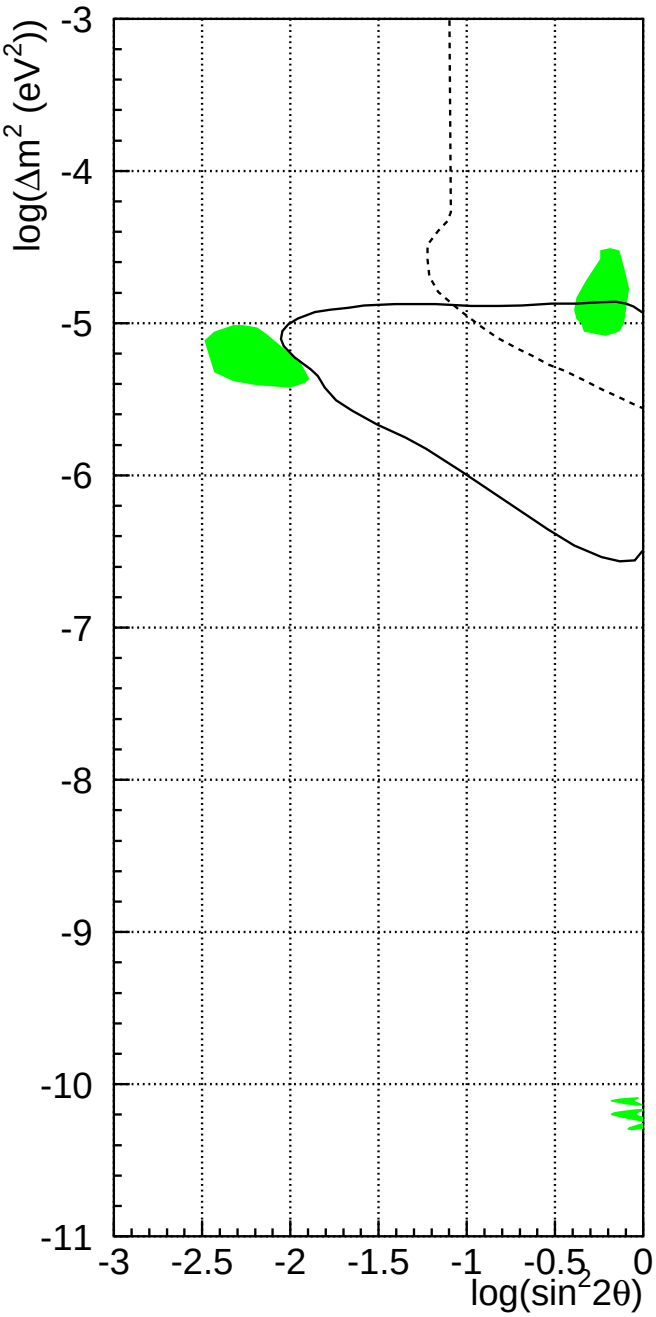

Figure 7: Three allowed regions in the $(\Delta m^2, \sin^2 2\theta)$ space (95 % CL) that explain the five experimental results (shaded regions). The SSM neutrino fluxes are those calculated by Bahcall and Pinsonneault [34]. The region enclosed by the solid curve is excluded from non-observation of the day-night effect by Super-Kamiokande. Analysis was made by Hata and Langacher [41]. Also indicated (dashed curve) is a sensitivity that one would obtain from 5-year operation of the Kam-LAND experiment [4] (see chapter 4 for details).

periments are of the disappearance type, namely try to detect possible oscillatory change or in general a decrease in the neutrino flux as the distance between reactor and detector is varied. Reaction that takes place in a detector is the neutrino capture,

$$\overline{\nu_e} + p \rightarrow e^+ + n, \tag{11}$$

in which p is a hydrogen nucleus in the target. Neutrino oscillations change the positron yield by the following expression ;

$$\frac{dN}{dT_e} = N_t \phi_\nu(E_\nu, L)\sigma(E_\nu) \times$$
$$\times \left[1 - \sin^2 2\theta \sin^2\left(1.27\frac{\Delta m^2 L}{E_\nu}\right)\right], \tag{12}$$

where T_e is the positron kinetic energy,

$$T_e = E_\nu - 1.8\,\mathrm{MeV}, \tag{13}$$

and ϕ_ν is the neutrino flux at the detector located at a distance L from the reactor,

$$\phi_\nu(E_\nu,\, L) \approx \phi_0(E_\nu)/4\pi L^2. \tag{14}$$

Δm^2, L and E_ν are in units of eV^2, m and MeV, respectively.

Experiments have so far been carried out with $L \leq$ a few 100 m. Unfortunately no evidence for the neutrino oscillation has been detected and only excluded regions in $(\Delta m^2, \sin^2 2\theta)$ space has been obtained.

Reactor neutrino experiments are still active and two km-long baseline experiments, Chooz [30] and Palo Verde [31], are expected to produce the first results in 1998. These two experiments were stimulated by the small ν_μ/ν_e ratio observed in atmospheric neutrinos. They would see a clear oscillation effect if the $\nu_e \rightarrow \nu_i$ $(i = \mu, \tau, sterile)$ oscillation is indeed the cause of the atmospheric neutrino anomaly. Even a 100km-scale experiment, Kam-LAND [4] has been funded and will begin data taking in 2000. It uses the old Kamiokande site, which is 2,700 m.w.e. deep underground and therefore the cosmic-ray muon flux is $10^4 \sim 10^5$ times lower than the previous experiments. Kam-LAND will detect neutrinos coming from a number of commercial power plants located between 150 and 210 km in Japanese main island, and their total thermal power amounts to 127 GW! The detector adopts 1,000 t liquid scintillator doped with Gd for efficient detection of neutrons (cf. eq(11)).

Table 9 shows some characteristics of the reactor experiments. Bugey [26] and Krasnoyarsk [27] experiments have already published their results. We have already shown in Fig.8 the excluded regions obtained by Bugey and Krasnoyarsk together with expected sensitivities of Chooz, Palo Verde and Kam-LAND. Also shown is an allowed region given by Kamiokande under the assumption that the atmospheric neutrino anomaly be caused by the $\nu_e - \nu_\mu$ oscillation. Kam-LAND is so much sensitive that its expected range extends down to several $\times 10^{-6}\mathrm{eV}^2$ and covers the MSW large-angle solution completely. See Fig.7. It will therefore shed new light on the solar neutrino problem.

Table 9: Some characteristics of existing and future reactor experiments

Experiments	Power (GW)	Detector	L(m)	E_ν. Rate /BG(d^{-1})	Ref.
Bugey	2.8	Liq.Sci (^{6}Li)[a]	15, 40, 95		[26]
Krasnoyarsk	—	^{3}He n-counters	57, 57.6, 231.4		[27]
Chooz	8.4	Liq.Sci (Gd) (4.8 t)	1,025	31/4	[30]
Palo Verde	10.9	Liq.Sci (Gd) (12 t)	740, 850	51/9 $\sim$ 79	[31]
Kam-LAND	127	Liq.Sci (Gd) (1,000 t)	150 $\sim$ 210 km	2/?	[4]

[a]Liquid Scintillator with ^{6}Li doped

5 Double Beta Decay

Element ^{76}Ge has extensively been used to search for double beta decay. Neighboring elements of ^{76}Ge have the following spin-parity and energy levels (J^P, E); $^{76}_{32}\mathrm{Ge}(0^+, 2.04\,\mathrm{MeV})$, $^{76}_{33}\mathrm{As}(2^-, 2.97\,\mathrm{MeV})$, $^{76}_{34}\mathrm{Se}(0^+, 0)$, where the lightest isobar is ^{76}Se. Beta decay of ^{76}Ge to ^{76}As is energitically forbidden. Hence ^{76}Ge has a very long halflife as it can only decay via second-order weak interactions, namely double beta decay;

$$^{76}\mathrm{Ge} \rightarrow ^{76}\mathrm{Se} + 2e^- + 2\overline{\nu_e}. \tag{15}$$

This decay mode is called $2\nu\beta\beta$ decay. If the electron-neutrino has a finite mass and is of the Majorana type [a], the neutrinoless double beta-decay ($0\nu\beta\beta$) could occur;

$$^{76}\mathrm{Ge} \rightarrow ^{76}Se + 2e^-. \tag{16}$$

The $0\nu\beta\beta$ decay has larger phase-space (proportional to the fifth power of the Q-value) than $2\nu\beta\beta$, and hence would decay much faster.

A halflife of $0\nu\beta\beta$ decay is given as [42]

$$T_{1/2} < m_\nu >^2 = \frac{m_e^2}{G_1 |M^{0\nu}|^2}, \tag{17}$$

$$< m_\nu > = \sum \varepsilon_i |U_{ei}|^2 m_i, \tag{18}$$

where G_1 is the phase-space factor, $M^{0\nu}$ the nuclear matrix element, ε_i the relative phase of the $i-th$ neutrino species, U_{ei} the mixing matrix in the neutrino sector, and m_i the

[a]If the weak interaction possesses a right-handed coupling, the $0\nu\beta\beta$ decay takes place without help of the finite neutrino mass. Hence the existence of the $0\nu\beta\beta$ decay does not guarantee that the neutrino has a finite mass.

Table 10: Q-values, phase-space factors G_1 and $T_{1/2} < m_\nu >^2$ for several candidate elements. [49]

	^{76}Ge	^{82}Se	^{100}Mo	^{130}Te	136Xe
J^P	0^+	0^+	0^+	0^+	0^+
Q(MeV)	2.041	2.995	3.034	2.533	2.479
$G_1(10^{-13}y^{-1}fm^2)$	6.70	30.63	57.60	66.40	72.79
$T_{1/2} < m_\nu >^2$ $(10^{24}\text{yr}\cdot\text{eV}^2)$					
Haxton et al[44]	1.7	0.58	—	0.16	—
Engel et al[45]	2.3	0.92	—	0.24	—
Engel et al[46]	14	5.6	1.0	0.66	3.3
Tomoda[47]	2.1	0.61	0.26	0.54	1.4
Staudt et al[48]	2.3	0.60	1.3	0.49	2.2

Table 11: Current lower limits on halflives of $0\nu\beta\beta$ decays and upper limits on $< m_\nu >$.
The $< m_\nu >$ limits are obtained based on the calculations of $T_{1/2} < m_\nu >^2$ given in table 10.

	^{76}Ge	^{82}Se	^{100}Mo	^{130}Te	^{136}Xe
Lower limits $T_{1/2}\,(10^{24}\text{yr}, 68\%\,\text{CL})$					
	11^a	0.027^b	0.044^c	0.028^d	0.79^e
Upper limits $< m_\nu >$ (eV, 68 %CL)					
Engel et al	1.1	1.4	4.8	4.9	2.0
Tomoda	0.44	4.8	2.4	4.4	1.3
Staudt et al	0.46	4.7	5.4	4.2	1.7

[a] Heidelberg-Moscow	19.2 kg 86%-enriched ^{76}Ge,	28.7 kg·yr	[3]
[b] UCI, TPC	45 g enriched ^{82}Se,	21,924 hr	[50]
[c] Osburn, Si(Li)	60.63 g 97%-enriched ^{100}Mo,	3,849.5 hr	[51]
[d] Milano, Bolometer	334 g TeO_2	9,234 hr	[52]
[e] St. Gotthard	62.5 %-enriched ^{136}Xe (1.46×10^{25} atoms)		[53]

neutrino mass ($i = 1, 2, 3$). Once the right-hand side of eq(17) is calculated and the halflife is measured, the neutrino mass $< m_\nu >$ can then be derived. Table 10 gives some relevant information on the $0\nu\beta\beta$ decay. Note that theoretical estimates of $|M^{0\nu}|^2$ have a large spread, about an order of magnitude, especially for ^{76}Ge. Hence it is important to use a variety of candidate elements in order to avoid an unexpected bias in the $|M^{0\nu}|^2$ calculations.

Unfortunately no new result has been reported on $T_{1/2}$. The current status on the lower limits of $T_{1/2}$ is tabulated in table 11. The upper limit on $< m_\nu >$ has reached 1ėV.

The Heidelberg-Moscow group [3] will continue the search with enriched ^{76}Ge detectors and will reach the sensitivity limit of $5 \times 10^{25}\,\text{yr}\,(< m_\nu >= 0.2 \sim 0.5\,\text{eV})$ by the year 2000. A new detector called NEMO3 [43] is under construction. It consists of 6180 drift cells with a gas mixture of He + 2 % C_2H_5OH and 1940 scintillation counters. Sources that will be inserted are 10 kg ^{100}Mo, 1 kg ^{82}Se and 1 kg ^{130}Te. The experimental sensitivity will eventually reach 10^{25} yr with 10 kg ^{100}Mo, which is equivalent with $< m_\nu >= 0.16 \sim 0.36\,\text{eV}$.

Table 12: Δm^2 and $\sin^2 2\theta$ inferred from atmospheric and solar neutrino anomalies. Associated errors are crude estimates.

	$\Delta m^2(\mathrm{eV}^2)$	$\sin^2 2\theta$	Remarks
Atmospheric neutrinos	$(5\overset{\times}{\div}3)\times 10^{-3}$	$0.7\sim 1$	
Solar neutrinos	$(1\overset{\times}{\div}2)\times 10^{-5}$	$\begin{cases} 0.2\sim 0.8 \\ 0.003\sim 0.01 \end{cases}$	large angle solution small angle solution
	$(5\sim 9)\times 10^{-11}$	$0.6\sim 1$	vacuum solution

6 Discussion and Conclusions

I have summarized the current status of nonaccelerator-based neutrino physics; atmospheric neutrinos, solar neutrinos, reactor neutrinos and double beta-decay. I did not discuss Tritium beta decay and ultra high-energy astrophysical neutrinos, because of limited time allocated to me. They may well become major topics in coming conferences.

As I discussed in the previous chapters, if the neutrino oscillation is indeed a culprit of atmospheric and solar neutrino anomalies, the present status on Δm^2 and $\sin^2 2\theta$ may be summarized as given in table 12.

It is tempting to speculate that the atmospheric neutrino anomaly is governed by m_3 and m_2 while the solar neutrino anomaly by m_2 and m_1. Then one may think of the following two scenarios: (i) Hierarchical mass sequence, $m_1 \ll m_2 \ll m_3$, in which, according to table 12, m_3 and m_2 are given approximately $7^{+5}_{-3}\times 10^{-2}\,\mathrm{eV}$ and $3^{+2}_{-1}\times 10^{-3}\,\mathrm{eV}$, respectively. m_1 should be much smaller. These masses are obviously too small for neutrinos to constitue dark matter in the Universe. Big Bang may have left a great number of neutrinos in the Universe, but, according to this scenario, they did not play a major role during the cosmic structure formation. (ii) Degenerate mass sequence, $m_1 \approx m_2 \approx m_3$, in which one can only say that $m_3 \geq 0.1\,\mathrm{eV}$. The masses could be as large as a few eV. Neutrinos are then heavy enough to have initiated the large-scale structure in the Universe. Double beta decay experiments are on the verge of ruling this scenario out (see table 11). However, this constraint can be evaded if neutrinos are of the Dirac type. The only hope would then be the tritium beta decay experiment with a mass resolution of 1 eV.

Acknowledgments

I received latest information from various experimental groups. I am grateful to B. Barish and D. Michael for MACRO, M. Goodman for Soudan 2, V. Gavrin for SAGE, T. Kirsten for GALLEX, R. Raghavan for Borexino, A. McDonald for SNO, F. Boehm for St. Gotthard and Palo Verde, R. Steinberg and H. Sobel for Chooz, A. Suzuki for Kam-LAND, H. Klapdor-Kleingrothaus for Heidelberg-Mascow, F. Piquemal, D. Lalanne and S. Jullian for NEMO3, K. Kume for ELEGANT, C. Spiering for Baikal, F. Halzen, C. Spiering and S. Barwick for AMANDA and E. Otten for the Mainz Tritium spectrometer. I enjoyed to talk with R. Raghavan, H. Fritzsch, C. Spiering, G. Heinzelmann, A. Suzuki, Y. Suzuki, B. Barish and A. Wagner. I thank the symposium organizers for an excellent and enjoyable symposium.

References

1. Mainz experiment, Ch. Weinheimer etal., *Phys. Lett.* B **300**, 210 (1993); A. Picard etal., *Z. Phys.* C **342**, 71 (1992).
2. Troitsk experiment, A.I. Belesev etal., *Phys. Lett.* B **350**, 263 (1995).
3. See *Double-Bata Decay*, Proceedings of the International Workshop held at European Center for Theoretical Studies, ed. by H. V. Klapdor-Kleingrothaus, pub. by World Scientific. 1996; H.V. Klapdor-Kleingrothaus, talk given at the International Conference on Beyond the Desert '97.
4. A. Suzuki (Tohoku University), private communication.
5. K.S. Hirata etal.,*Phys. Lett.* B **205**, 416 (1988); *Phys. Lett.* B **280**, 146 (1992); Y. Fukuda etal., *Phys. Lett.* B **335**, 237 (1994).
6. M. Aglietta etal. *Europhys. Lett.* **8**, 611 (1989).
7. Ch. Berger etal., *Phys. Lett.* B **227**, 489 (1989); *Phys. Lett.* B **245**, 305 (1990); K. Daum etal., *Z. Phys.* C **66**, 417 (1995).
8. D. Casper etal., *Phys. Rev. Lett.* **66**, 2561 (1991); R. Becker-Szendy etal., *Phys. Rev.* D **46**, 3720 (1992).
9. W.W.M. Allison etal., *Phys. Lett.* B **391**, 491 (1997). M. Goodman, private communication.
10. S. Ahlen etal., *Nucl. Inst. Meth.* A **234**, 337 (1993); M. Ambrosio etal., *Phys. Lett.* B **357**, 481 (1995).
11. B.T. Cleveland etal., *Nucl. Phys. (Proc. Suppl.)* B **38**, 47 (1995); R. Davis, *Prog. Part. Nucl. Phys.* **32**, 13 (1994).
12. K. S. Hirata etal., *Phys. Rev. Lett.* **65**, 1297 (1990); *Phys. Rev.* D **44**, 2241 (1991).
13. J. N. Abdurashitov etal., *Phys. Lett.* B **328**, 234 (1994); V.N. Gavrin, private communication.
14. P. Anselmann etal., *Phys. Lett.* B **327**, 377 (1994); *Phys. Lett.* B **357**, 237 (1995); W. Hampel etal., *Phys. Lett.* B **388**, 384 (1996).
15. Y. Totsuka, ICRR-Report-227-90-20.
16. G. Ewan, *Nucl. Inst. Meth* A **314**, 373 (1992); *Physics in Canada* **48** 112 (1992); A. B. McDonald, in *Proceedings of Neutrino 96*, Helsinki, 1996.
17. Borexino Collaboration, *Proposal for a Real Time Detector for Low Energy Solar Neutrinos* (1991).
18. Baikal Collaboration, DESY 97-033.
19. F. Halzen, preprint astro-ph/9605014, MADPH-96-937.
20. G. Barr, T.K. Gaisser and T. Stanev, *Phys. Rev.* D **39**, 3532 (1989), V. Agrawal etal., *Phys. Rev.* D **53**, 1314 (1996); calculations have been updated several times.
21. M. Honda etal., *Phys. Lett.* B **248**, 193 (1990); *Phys. Rev.* D **52**, 4985 (1995); calculations have been updated several times.
22. T.K. Gaisser etal., *Phys. Rev.* D **54**, 5578 (1996).
23. Super-Kamiokande collaboration, to be published.
24. Kamiokande collaboration, to be published.
25. M. Glück, E. Reya and A. Vogt, *Z. Phys.* C **67**, 433 (1995).
26. B. Achkar etal., *Nucl. Phys.* B **434**, 503 (1995).

27. G. S. Vidyakin etal., *Sov. Phys. JETP* **71**, 424 (1990); *JETP Lett.* **59**, 390 (1994).
28. W. Frati etal., *Phys. Rev.* D **48**, 1140 (1993).
29. R. Becker-Szendy etal., *Phys. Rev. Lett.* **69**, 1010 (1992).
30. Chooz collaboration, *Proposal to Search for Neutrino Vacuum Oscillations to* $\Delta m^2 = 10^{-3}\mathrm{eV}^2$ *Using a 1 km Baseline Reactor Neutrino Experiment*; June 1993; in http://duphy4.physics.drexel.edu/chooz-pub/index.html; R. Steinberg, private communication.
31. Palo Verde collaboration, *Palo Verde Neutrino Oscillation Experiment* http://www.cco.caltech.edu/ songhoon/Palo-Verde/thesis.html.
32. H. Shibahashi and M. Takata, *Publ. Astron. Soc. Japan* **48**, 377 (1996); M. Takita and H. Shibahashi, *'Solar Models Based on Heioseismology and the Solar Neurino Problem'* submitted to *Ap. J.* (Aug, 1997).
33. B. Ricci etal., *Phys. Lett.* B **407**, 155 (1997).
34. J.N. Bahcall and M.H. Pinsonneault *Rev. Mod. Phys.* **67**, 781 (1995).
35. W. Hampel etal., *Phys. Lett.* B **388**, 384 (1996).
36. J.N. Abdurashitov etal., *Phys. Rev. Lett.* **77**, 4708 (1996).
37. A. Cumming and W.C. Haxton, *Phys. Rev. Lett.* **77**, 4286 (1996).
38. J.N. Bahcall and M.H. Pinsonneault, *Phys. Rev. Lett.* **78**, 171 (1997).
39. L. Wolfenstein, *Phys. Rev.* D **17**, 2369 (1978); *Phys. Rev.* D **20**, 2634 (1979); S.P. Mikheyev and A.Yu. Smirnov, *Sov. J. Nucl. Phys.* **42**, 913 (1985); *Nuovo Cimento* **9C**, 17 (1986).
40. S.L. Glashow and L.M. Krauss, *Phys. Lett.* B **190**, 199 (1987).
41. N. Hata and P. Langacker, IASSNS-AST 97/29, UPR-751T, hep-ph/9705339, May 1997.
42. See theoretical papers in ref [3].
43. D. Dassié etal., *Phys. Rev.* D **51**, 2090 (1995); R. Arnold etal., *Z. Phys.* C **72**, 239 (1996); S. Julllian, talk given at the International workshop on Double Beta Decay and Related Topics in Trento, April 24 – May 5, 1995.
44. W.C. Haxton and G.J. Stephenson, *Prog. Part. Nucl. Phys.* **12**, 409 (1984).
45. J. Engel etal., *Phys. Lett.* B **225**, 5 (1989).
46. J. Engel, P. Vogel and M.R. Zirnbauer *Phys. Rev.* C **37**, 731 (1988).
47. T. Tomoda, *Rep. Prog. Phys.* **54**, 53 (1991).
48. A. Staudt, K. Muto and H.V. Klapdor-Kleingrothaus, *Europhys. Lett.* **13**, 31 (1990).
49. This table was made referring to table 3 in page 330 of ref [3] by P. Vogel.
50. S. R. Elliot etal., *Phys. Rev.* C **46**, 1535 (1992).
51. M. Alson-Garnjost etal., *Phys. Rev. Lett.* **71**, 831 (1993).
52. M. Alessandrello etal., *Phys. Lett.* B **335**, 519 (1994).
53. J.-C. Vuilleumier etal., *Phys. Rev.* D **48**, 1009 (1993); K. Lou etal., in *Proceedings of Yamada Conference 1995*, World Scientific p.192, 1995.
54. S. Kasuga etal., *Phys. Lett.* B **374**, 238 (1996).